Optimal Time Delay Extraction for Transmission Line Modeling

Bjørn Gustavsen, *Fellow*, *IEEE*

Abstract—Frequency-dependent transmission line modeling by the traveling wave method requires to approximate the propagation function with a delayed rational function. Some approaches are based on modal decomposition where scalar functions are fitted with a rational model plus a single time delay. The delay is calculated from the modal velocity and the minimum-phase-shift (mps) angle which can be reconstructed from the magnitude function. This paper shows that the accuracy in the phase reconstruction as calculated by Bode's magnitude-phase integral relation can be greatly improved by removal of a singularity in the integrand, and by prediction of out-of-band samples for the magnitude derivative. It is further shown that the time delay giving the smallest RMS-error in the final rational approximation is often substantially larger than the mps induced delay. An improved estimation is calculated via an auxiliary magnitude function and used for determining a bracketing interval for the true optimum which is identified by searching.

Index Terms—Transmission line model, frequency dependent, minimum phase shift, delay calculation.

I. INTRODUCTION

THE simulation of electromagnetic transients in high-voltage power systems is usually based on EMTP-type simulation tools [1]. The most suitable transmission line model for representing overhead lines and underground cables is usually the frequency-dependent traveling wave model which decomposes voltages and currents at the two line ends into forward and backward propagating waves. Here, the transmission line is described [2],[3] by its characteristic admittance (impedance) which defines the relation between voltage waves and current waves, and the propagation function which defines the distortion and delay of a wave as it travels between the two line ends. The characteristic admittance and propagation function are fitted in the frequency domain by rational functions, thereby allowing efficient time domain simulation via recursive convolution [4].

The earliest traveling wave models were formulated within a modal framework where each mode (eigenvalue) is effectively represented by a single-conductor transmission line, again represented by a frequency-dependent traveling wave model [4],[5]. The frequency-dependent modal transformation matrix is approximated by a real and constant matrix, thereby introducing a modeling error. With some cable systems, the frequency dependency can be taken into account by introducing another convolution [6],[7].

The accuracy limitations imposed by the assumption of a real and constant transformation matrix has led to the development of traveling wave models directly in the phase (physical) domain without residing to modal decomposition. With the Universal Line Model (ULM) [8],[9], rational fitting of modal components is still used as an intermediate step in the modeling of the propagation function.

With both the modal domain and phase domain models (ULM), it is necessary to fit each modal component of the propagation function with a delayed rational function. The calculation can be performed using J. Marti's asymptotic fitting method [5] of the propagation magnitude function followed by a time delay optimization. More accurate results are obtained by application of vector fitting (VF) [10],[11]. Here, it is necessary to pre-calculate the time delay to be used prior to application of VF. In [7] it was proposed to calculate the delay at a single frequency using as information the modal velocity at that frequency and the minimum-phase-shift (mps) angle associated with the magnitude function of the propagation function. The background for the mps angle calculation in [7] is related to Bode's work but no details were shown. In [12] it was shown that the accuracy of the mps angle could be greatly improved by a direct implementation of a formula that appeared in Bode's original work .

In this paper, the formula used in [7] is derived, showing that it stems from the original Bode formulae but modified to remove a singularity in the integrand so as to improve its accuracy when evaluating the integral discretely. In addition, an error existing in the presented formula [7] is corrected. The resulting formula is compared against the result by direct evaluation of Bode's formula for a synthetic example, and the significance of integration limits and frequency resolution is investigated. Errors due to the upper integration limit are reduced by calculating out-of-band samples using a polynomial prediction model. Next, it is shown by application to a single-conductor line that the mps-delay is generally too small when the objective is to find a rational approximation with the smallest RMS-error. An improved estimation approach is introduced based on an auxiliary magnitude function, and a search procedure is proposed based on the ideas in [14], for finding the optimal time delays. Finally, the approach is demonstrated for the modeling of a cable system.

II. Time Delay And Minimum Phase-Shift Function

Consider a single conductor transmission line (or a mode of a multi-conductor line) with per-unit-length series impedance Z and shunt admittance Y. The modeling of the line by the traveling wave methods requires to calculate a rational model approximation of the propagation function

$$H(\omega) \cong \left(\sum_{m=1}^{N} \frac{r_m}{j\omega - a_m} \right) e^{-j\omega\tau} \tag{1}$$

To calculate the rational model (1), it is necessary to first estimate the time delay τ so that the rational factor of (1) can be obtained by standard techniques (e.g. VF [10],[11]) by solving the least-squares problem

$$H(\omega) e^{j\omega\tau} \cong \sum_{m=1}^{N} \frac{r_m}{j\omega - a_m} \tag{2}$$

It was shown in [7] that the time delay can be calculated as

$$\tau = \frac{l}{v(\omega)} + \frac{\varphi_{mps}(\omega)}{\omega} \tag{3}$$

where φ_{mps} denotes the minimum-phase-shift (mps) angle of the magnitude function of the propagation function, $|H(\omega)|$. $v(\omega)$ and l denote the propagation velocity and line length, respectively. The second term in (3) approaches zero with increasing frequency, implying that the delay in (3) is also the lossless delay, $\tau = \tau_\infty$.

In principle, any single frequency ω can be used for determining τ by (3). In the implementation [9], the delay was evaluated at the frequency point where the magnitude function had decayed to a value equal to the target error for the RMS-error.

III. Phase Reconstruction From Magnitude Data

A. Bode's Method

Bode has shown [13] that the mps function φ_{mps} at frequency ω_k can be calculated from the magnitude function using the formula

$$\varphi_{mps}(\omega_k) = \frac{1}{\pi} \int_{-\infty}^{\infty} \frac{d \log |H|}{du} \log \left(\coth \frac{|u|}{2} \right) du \tag{4}$$

where

$$u = \log \left(\frac{\omega}{\omega_k} \right) \tag{5}$$

This method (4) was used in [12].

B. Removal of Singularity

One challenge with the direct evaulation of (4) using discrete samples is that u in (5) approaches zero when $\omega \to \omega_k$, thereby causing $\coth(\cdot)$ to undergo a fast variation while approaching infinity. In order to alleviate this difficulty, the integrand in (4) can be modified such that the factor in front of the log-term approaches zero when $\omega \to \omega_k$. To see how this is done, consider the simplified problem of solving

$$\int_{-\infty}^{\infty} f(x) g(x) dx \tag{6}$$

where $g(x)$ approaches infinity at some point x_0. This problem can be handled by solving the alternative problem

$$\int_{-\infty}^{\infty} f(x) g(x) dx = \int_{-\infty}^{\infty} (f(x) - f(x_0)) g(x) dx + f(x_0) \int_{-\infty}^{\infty} g(x) dx \tag{7}$$

provided that a closed form solution exists for the rightmost integral in (7).

For (4) one can write

$$\varphi_{mps}(\omega_k) = \frac{1}{\pi} \int_{-\infty}^{\infty} \left[\frac{d \log |H|}{du} - \frac{d \log |H|}{du} \bigg|_{\omega_k} \right] \log \left(\coth \frac{|u|}{2} \right) du$$

$$+ \frac{1}{\pi} \frac{d \log |H|}{du} \bigg|_{\omega_k} \int_{-\infty}^{\infty} \log \left(\coth \frac{|u|}{2} \right) du$$

$$\tag{8}$$

The last integral factor (second line) in (8) can be evaluated analytically utilizing the relation [13]

$$\int_{-\infty}^{\infty} \log \left(\coth \frac{|u|}{2} \right) du = \frac{\pi^2}{2} \tag{9}$$

It follows that (8) can now be evaluated as

$$\varphi_{mps}(\omega_k) = \frac{\pi}{2} \frac{d \log |H|}{du} \bigg|_{\omega_k} + \Delta(u) \tag{10a}$$

where

$$\Delta(u) = \frac{1}{\pi} \int_{-\infty}^{\infty} \left[\frac{d \log |H|}{du} - \frac{d \log |H|}{du} \bigg|_{\omega_k} \right] \log \left(\coth \frac{|u|}{2} \right) du \tag{10b}$$

Note that the result (10b) was presented in [16] without derivation where it incorrectly used absolute values for the two terms inside the square brackets. The (incorrect) formula was included in [7] and later works, and also found its way into the ULM implementation. In [12], the correct form (10b) was used but with a different approach for the derivation.

IV. Numerical Evaluation

Using the discretization scheme in [14], one obtains for the band-limited evaluation of (10) with $N_{\omega-1}$ frequency samples the expression

$$\varphi_{mps}(\omega_k) \cong \frac{\pi}{2} A_k + \frac{1}{\pi} \sum_{j=1}^{N_{\omega-1}} \left(A_j - A_k \right) B_j \log(\omega_{j+1} / \omega_j) \tag{11a}$$

where

$$A_j = \frac{\log(|H_{j+1}| / |H_j|)}{\log(\omega_{j+1} / \omega_j)}, \quad A_k = \frac{\log(|H_{k+1}| / |H_k|)}{\log(\omega_{k+1} / \omega_k)} \tag{11b}$$

$$B_j = \log(\coth\left(\frac{1}{2}\left|\log(\frac{\omega_j + \omega_{j+1}}{2\omega_k})\right|\right)) \qquad (11c)$$

Direct evaluation of Bode's formula (4) using a ditto discretization scheme gives

$$\varphi_{mps}(\omega_k) \cong \frac{1}{\pi}\sum_{j=1}^{N_\omega-1} A_j B_j \log(\omega_{j+1}/\omega_j) \qquad (12)$$

V. SYNTHETIC EXAMPLE

A. Frequency Response

To see the advantage of phase reconstruction using (11) over the direct approximation of (12), both methods are applied to a synthetic frequency response,

$$H(\omega) = K\frac{(j\omega - z_1)(j\omega - z_2)\cdots(j\omega - z_8)}{(j\omega - p_1)(j\omega - p_2)\cdots(j\omega - p_9)}e^{-j\omega\tau} \qquad (13)$$

This example has been adapted from [12] with τ=407.6 µs, K=41123.67 and poles and zeros listed in Table I. It is observed that all poles and zeros lie in the left half plane. Therefore, $H(\omega)$ is a mps function when τ=0. Fig. 1 shows the magnitude function in the range 1 Hz-100 MHz, with 20 samples per decade of frequency.

TABLE I.
POLES AND ZEROS IN (13).

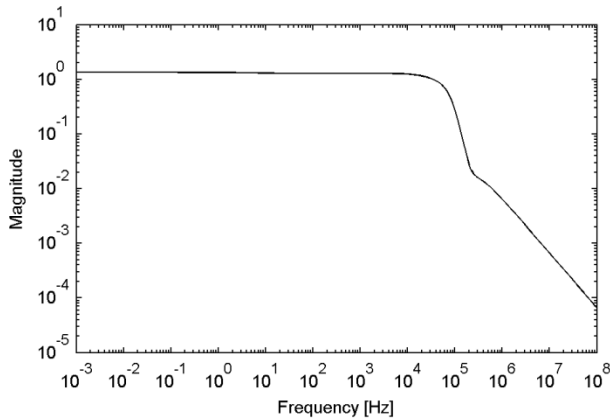| p	z
-2.13	-2.14
-12.80	-12.98
-71.39	-73.65
-229737.95	$-177.22 \pm j364.70$
$-177.53 \pm j365.86$	$-491141.78 \pm j1261050.84$
$-264211.31 \pm j430308.14$	

Fig. 1. Magnitude function of H.

B. Phase Reconstruction

Fig. 2 shows the associated phase angle of $H(\omega)$ when τ=0. as well as the phase angle reconstructed from the magnitude function $|H(\omega)|$ using either direct calculation (12) or singularity removal (11). The phase reconstruction is performed by repeatedly applying (11) and (12) with k varied between the first and second last sample. All available samples are used in the calculation, with 20 samples per decade of frequency. It is observed that the direct application leads to higher errors. The improvement of using the singularity removal is highlighted in Fig. 3 which shows the deviation (absolute value) from the true angle.

The difference in phase angle reconstruction errors can be understood by considering the behavior of the two integrands of (11) and (12). Fig. 4 shows the two integrands with a very fine frequency resolution when the evaluation frequency ω_k is chosen where the magnitude function is 0.25 (104 kHz). It is observed that usage of singularity removal leads to the numerical evaluation of a more well-behaved integrand whereas direct evaluation gives an integrand with a sharp peak at the evaluation frequency.

With singularity removal, the error seems to approach zero at very high frequencies. This result occurs since in this example the magnitude function is almost linear in the loglog plot at frequencies above 1 MHz so that A_k and A_j are nearly equal. Therefore, $\Delta(u)$ in (11a) approaches zero so that only the constant term remains, which includes the effect from frequencies beyond the 100 MHz limit. It is to be noted that when fitting a propagation function, the magnitude function will not be linear on a log-log plot and so the error will not approach zero.
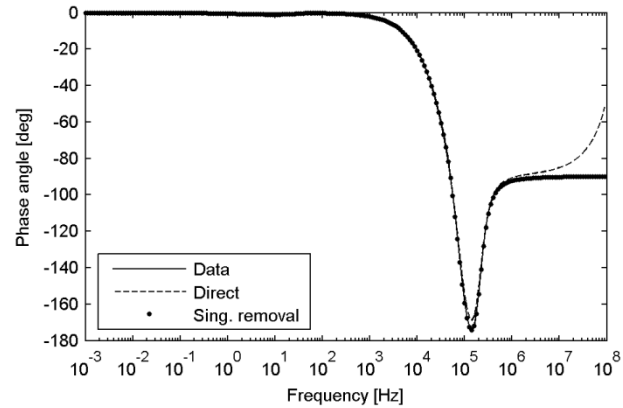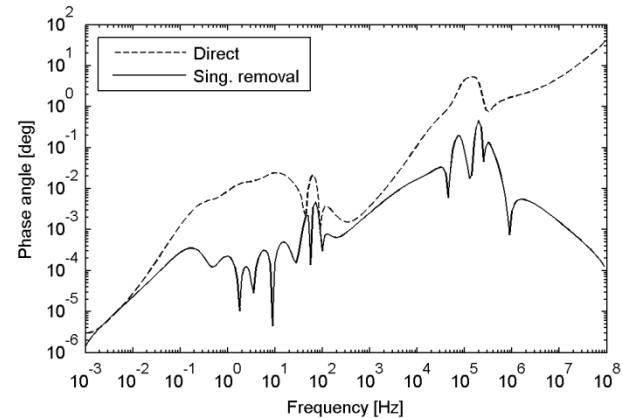

Fig. 2. Reconstructed phase angle.

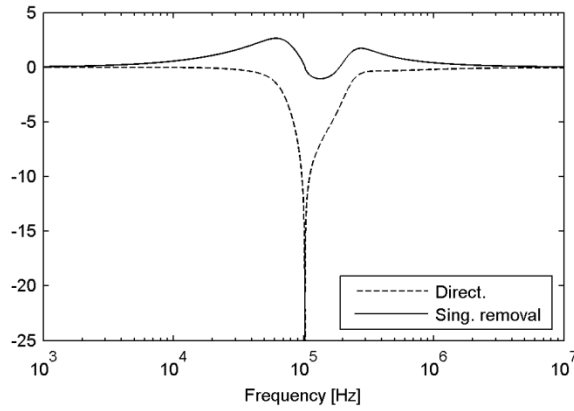Fig. 3. Error in reconstructed phase angle. (Logarithmic ordinate scale).

Fig. 4. Integrand with singularity removal (12) and direct evaluation (11).

C. Time Delay Removal and Fitting With Rational Functions

Using the same example, the phase reconstruction is again performed at a single evaluation frequency ω_k where the magnitude has decayed to 0.25, this time using four decades of frequency on each side of the evaluation point and 20 samples per decade. Following compensation with the time delay, the resulting frequency response is fitted using VF [10],[11] with N=10 poles.

The result in Table II shows that the improved accuracy in phase reconstruction by singularity removal leads to a more precise estimation of the time delay and thereby a smaller RMS-error of the final model.

Table III shows the RMS-error with alternative sampling resolutions. It is observed that singularity removal gives a consistently more accurate result as the RMS-error quickly drops with increasing sampling density. Finally, the sensitivity to the integration limits is shown in Table IV. Increasing the limit improves the accuracy, as expected.

TABLE II.
COMPARISON OF DELAY COMPUTATIONS.

	Correct solution	Singularity removal*	Direct evaluation*
φ_{mps} [deg]	−161.32	−161.33	−156.77
τ [µs]	407.60	407.59	407.72
RMS error	3.1E−14	2.5E−9	1.7E−3

*By using 4 decades and 20 logarithmic samples per decade. Point of evaluation chosen where |H|=0.25.

TABLE III.
DELAY COMPUTATIONS FOR ALTERNATIVE FREQUENCY RESOLUTIONS.

	RMS error	
Samples per decade	Singularity removal*	Direct evaluation*
5	5.2E−4	8.4E−3
20	2.5E−9	1.7E−3
100	1.1E−12	3.3E−4

*By using 4 decades. Point of evaluation chosen where |H|=0.25.

TABLE IV.
DELAY COMPUTATIONS FOR ALTERNATIVE INTEGRATION LIMITS.

	RMS error	
Decades	Singularity removal*	Direct evaluation*
1	6.5 E−4	3.1 E−3

2	9.9 E−5	1.8 E−3
3	6.2 E−7	1.7 E−3
4	2.5 E−9	1.7 E−3

*By using 20 logarithmic samples per decade. Point of evaluation chosen where |H|=0.25.

VI. EXTENSION OF INTEGRAL TO HIGHER FREQUENCIES

A. Unavailable Data at High Frequencies

With practical use of time delay identification schemes for transmission line modeling, one is usually given the frequency data within a limited band on a logarithmic base. At the same time, one will normally attempt to calculate φ_{mps} at a relatively high frequency where the modes are well-defined, which can truncate the upper frequency limit to be much less than four decades above the evaluation point. Another difficulty is that the strong attenuation of the ground mode may simply damp the magnitude function so much that it cannot be computed at high frequencies on a digital computer. This makes it necessary to restrict the upper frequency limit for such modes.

B. Predictive Model for Magnitude Derivatives

Consider that at a set of samples is available at logarithmically spaced frequencies $(\omega_1, \omega_2, \cdots \omega_N)$. The following is observed from (10) and (11)

1. The integrand is calculated based on derivate estimates of the magnitude function, formed by A_j and A_k while the magnitude function itself is not used.

2. The B_j term is constant as function on frequency due to the logarithmic spacing, as is also the factor $\log(\omega_{j+1} / \omega_j)$.

The derivatives needed for computing A_j beyond ω_N can be calculated using a predictive polynomial obtained from a few sample values in the neighborhood of ω_N. As an example, consider the use of a second order derivative prediction based on the last four samples $(\omega_i, |H_i|)$, $i=N−3$, $N−2$, $N−1$, N. From these samples, three derivative estimates are calculated for $i=N−3$, $N−2$, $N−1$,

$$\frac{d \log |H(\omega_i)|}{d \log \omega_i} \approx \frac{\log(|H(\omega_{i+1})| / |H(\omega_i)|)}{\log(\omega_{i+1} / \omega_i)} = A_i \quad (14)$$

From the derivative estimates (14), a second order predictive model (15) is established for calculating the derivatives at out-of-band samples ω_k,

$$\frac{d \log |H(\omega_k)|}{d \log \omega_k} \approx a + b \log \frac{\omega_k}{\omega_{N-3}} + c \left(\log \frac{\omega_k}{\omega_{N-3}}\right)^2 \quad (15)$$

The coefficients in (15) are found by solving the linear equation

$$\begin{bmatrix} 1 & 0 & 0 \\ 1 & \log\dfrac{\omega_{N-2}}{\omega_{N-3}} & (\log\dfrac{\omega_{N-2}}{\omega_{N-3}})^2 \\ 1 & \log\dfrac{\omega_{N-1}}{\omega_{N-3}} & (\log\dfrac{\omega_{N-1}}{\omega_{N-3}})^2 \end{bmatrix} \begin{bmatrix} a \\ b \\ c \end{bmatrix} = \begin{bmatrix} A_{N-3} \\ A_{N-2} \\ A_{N-1} \end{bmatrix} \qquad (16)$$

The extension to higher or lower orders is straightforward.

C. Example: Single Conductor Overhead Line

As an example we consider a 30-km single-conductor overhead line over a lossy ground as shown in Fig. 5. With a speed of light in vacuum of 300 m/µs, the lossless time delay is $\tau_\infty=100$ µs. The magnitude function is shown in Fig. 6.
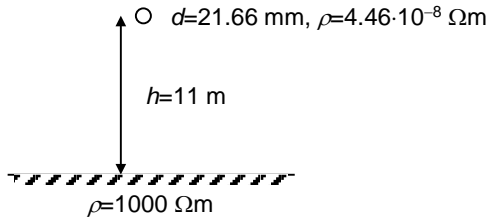

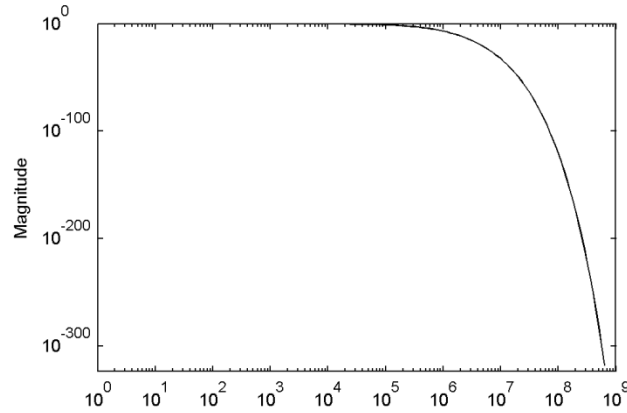Fig. 5. Single conductor overhead line. 30 km.

Fig. 6. Propagation function, $H(s)$.

Consider now that samples are available only up to 10 MHz. Fig. 7 reports the calculation of derivatives at frequencies above 10 MHz using predictive models with alternative orders. It is observed that better approximations are obtained as the model order is increased. The 2nd order approximation is the one by (15). For reference, truncation of the integral at 10 MHz implies an assumption of a 0th order model with the derivative being zero.
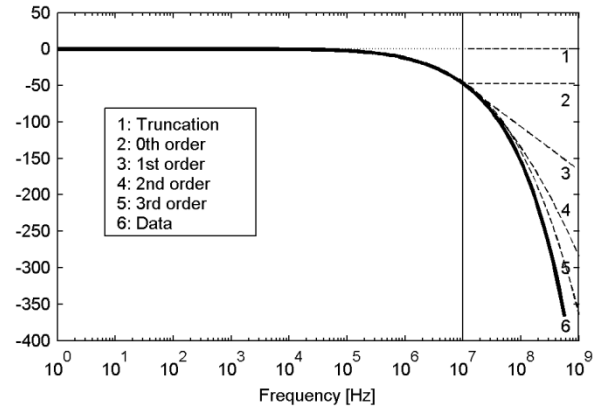

Fig. 7. Magnitude function derivative and model estimates above 10 MHz.

The effect of using the predicted derivatives is investigated next. It is assumed that samples are available only between 1 Hz and 10 MHz with 20 samples per decade. Derivative samples above 10 MHz are calculated using the third order predictor. All available samples are used in the phase reconstruction calculations.

Fig. 8 reports the relative error with respect to the correct time delay $\tau_\infty=100$ µs, which corresponds to speed of light in vacuum (300 m/µs). The errors are shown with alternative number of frequency decades above above 10 MHz. It is observed that using two or more decades with predicted derivatives makes the error decrease from about 1% to below 0.1%, for frequencies above 100 Hz.
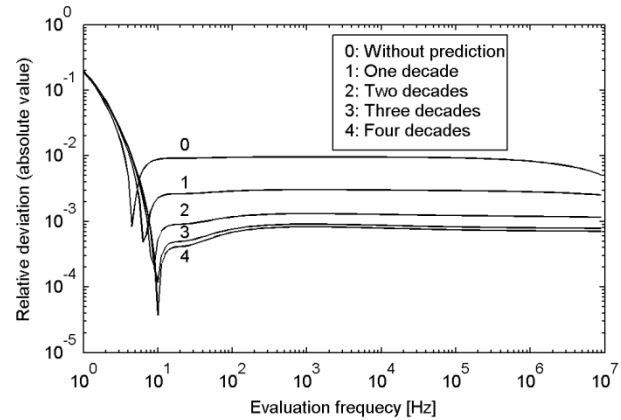

Fig. 8. Relative error in estimated delay vs. frequency point of evaluation. Parameter: additional decades with predicted derivatives.

VII. TIME DELAY OPTIMIZATION

Proper application of (11) produces a highly accurate estimation for the lossless delay of the line, i.e. the delay evaluated at infinite frequency. Often, however, the use of a larger delay will lead to a substantially more accurate fitting of the modes as demonstrated in [14].

Fig. 9 shows the RMS-error of the fitting error for $H(s)$ for the single conductor overhead line example, as function of the time delay used for compensation in (2). It is observed that the optimal time delay is larger than the lossless delay, and it is also dependent on the model order with lower orders implying larger delays.
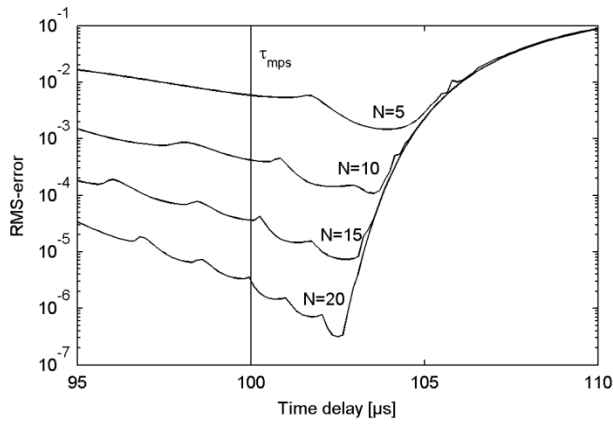
Fig. 9. RMS-error vs. model order.

Fig. 10. RMS error with golden section search. $N=20$. Parameter: Frequency ω_b for calculating right bracketing value.

A. Bracketing Interval for Optimization

The optimum delay τ^* can be found by searching in the neighborhood of the mps-delay. A reliable search algorithm can be obtained by first defining a bracketing interval $[\tau_a, \tau_b]$ for the optimum, followed by a suitable search method within the interval. Since one generally has $\tau^* > \tau_\infty$, the left limit can be taken as $\tau_a = \tau_\infty$, while the right limit remains to be determined. In [14] it was proposed to choose the right limit as

$$\tau_b = \frac{l}{v(\omega_b)} \tag{17}$$

where ω_b is the frequency where the magnitude function $|H(\omega)|$ has decayed to the target error for the rational approximation to be calculated, i.e. the magnitude of the complex deviation between the original H and its rational fit. This compensation gives zero phase angle for the compensated function at this frequency, $H(\omega_b)\exp(j\omega_b\tau)$, and is therefore guaranteed to be too large. Table V lists τ_b for the overhead line example, for alternative values of the evaluation frequency ω_b. It is observed that τ_b decreases towards the lossless delay $\tau_\infty = 100\,\mu s$ as ω_b increases.

TABLE V.
SENSITIVITY OF UPPER INTEGRATION LIMIT TO EVALUATION FREQUENCY

$\omega_b/(2\pi)$ [Hz]	$|H|$	τ_b [µs]
10^3	0.9648	121.41
10^4	0.73391	114.69
10^5	0.072897	108.61
10^6	$2.83E-8$	103.90
10^7	$7.30E-36$	101.39

B. Searching for the Optimum

With the bracketing interval known, the optimum can be found using simple search procedures. Fig. 10 reports the results from application of golden section search [17] with $\tau_a = 100\,\mu s$ and alternative values for ω_b. It is seen that the alternative searches quickly converge to the same result, with fastest convergence with a high value for ω_b due to the narrower search interval. All examples use $N=20$ poles. The optimum is obtained with $\tau^* = 102.52\,\mu s$.
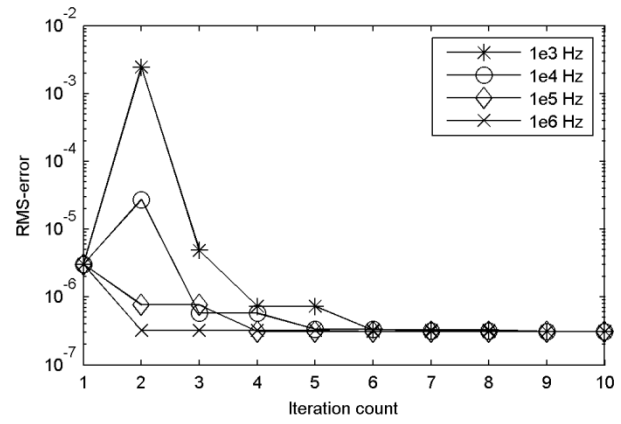
VIII. BRACKETING FOR SEARCH INTERVAL

A. Left Bracketing Using Lossless Delay

The use of the lossless delay (τ_∞) for representing the left interval bracketing can however be inappropriately small for modes with return in earth unless the external inductance is much larger than the internal inductance. To see this, consider again the overhead line in Fig. 5 but with alternative heights. Figs. 11 and 12 show respectively the magnitude and delay of the line propagation function $|H|$ as function of frequency. Fig. 13 shows the RMS-error of a fitting using $N=15$ poles. With 0.1 meter height, the optimal delay is $162\,\mu s$ which is much larger that the $100\,\mu s$ lossless delay.
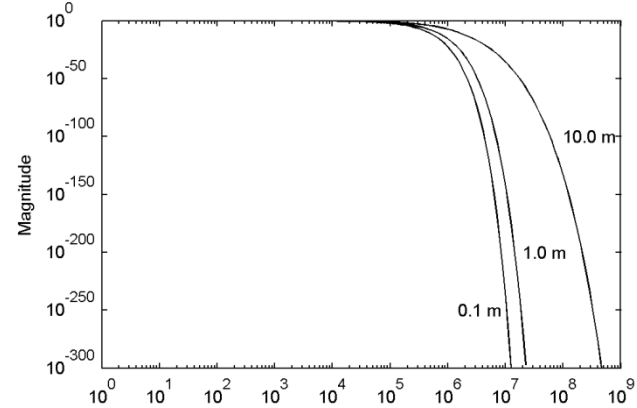

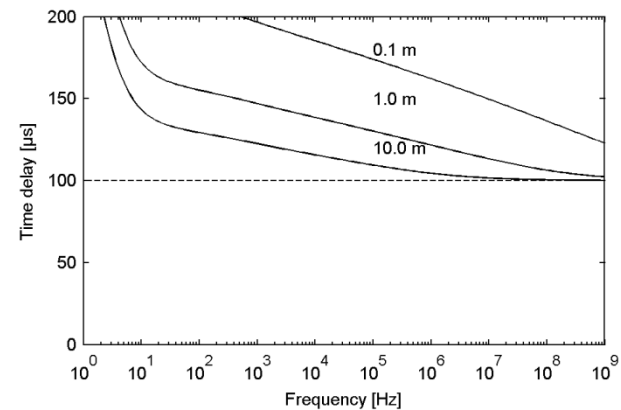Fig. 11. Magnitude of propagation function with alternative conductor heights.

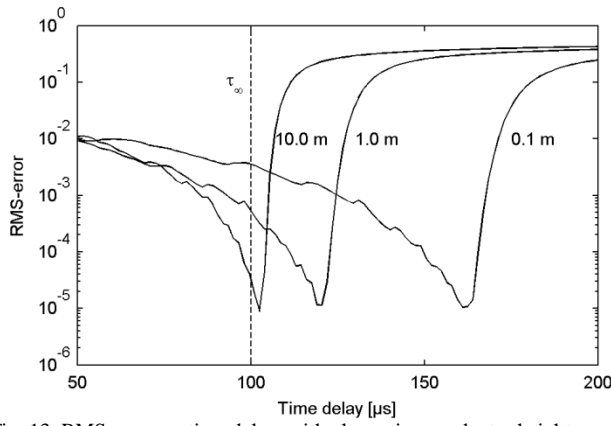Fig. 12. Propagation time delay with alternative conductor heights.

This article has been accepted for publication in a future issue of this journal, but has not been fully edited. Content may change prior to final publication. Citation information: DOI 10.1109/TPWRD.2016.2609039, IEEE Transactions on Power Delivery

7

Fig. 13. RMS error vs. time delay, with alternative conductor heights.

B. ULM Bracketing Approach Based on Specified Error Level

In the original implementation of the ULM and briefly outlined in [9], a target error ε is specified for the fitting of each mode and the model order is iteratively increased until this requirement is met. In each iteration, the optimal time delay is determined using optimization with the bracketing interval limits determined as follows.

The evaluation frequency ω_1 is selected as the frequency sample where the magnitude function $|H|$ is closest to the specified ε. In the case that $|H(\omega)|$ is greater than ε in the entire frequency range, ω_1 is selected as the highest frequency sample. The *right* bracket is chosen as $\tau_b = l / v(\omega_1)$ as mentioned in Section VII-A. The *left* bracket τ_a is evaluated at ω_1 using (3) with $\varphi_{mps}(\omega_1)$ calculated from the magnitude function. In principle, this approach produces the lossless delay, $\tau_a \cong \tau_\infty$ in Fig. 13.

C. Improved Estimation of Left Bracket

The left bracket delay can be improved by considering the largest phase angle that can be supported by a rational model of a given order N. A real-valued auxiliary function $h_{aux}(\omega)$ is introduced (18) which is equal to $|H(\omega)|$ at frequencies below the evaluation frequency ω_1. At frequencies above ω_1, $h_{aux}(\omega)$ is specified to decay with N decades per decade of frequency, which is the fastest magnitude decay that is achieveable with an Nth order model.

$$h_{aux}(\omega) = \begin{cases} |h(\omega)| & , \ \omega \le \omega_1 \\ |h(\omega_1)| \left(\dfrac{\omega_1}{\omega} \right)^N | & , \ \omega > \omega_1 \end{cases} \quad (18)$$

This is illustrated in Fig. 14 for an example with $N=4$ and $\omega_1 = 2\pi \cdot 10^5$ Hz. From the auxiliary magnitude function, a modified mps angle $\tilde{\varphi}_{mps}$ is evaluated at $\omega = \omega_1$ and used for determining the time delay $\tilde{\tau}_\infty$ by (3). The final delay to be used is chosen as

$$\tau = \max(\tilde{\tau}_\infty, \tau_\infty). \quad (19)$$

Fig. 15 shows the left and right interval for the bracketing interval for the example in Fig. 14 with $\tilde{\varphi}_{mps}$ calculated from

$|H_{\omega 1}(\omega)|$ by (11). The calculation assumed $\varepsilon = 10^{-5}$ and the parameter (N) denotes the resulting order. It is observed that the left bracket delay is larger than the lossless delay, leading to faster and more reliable searching for the optimum value.
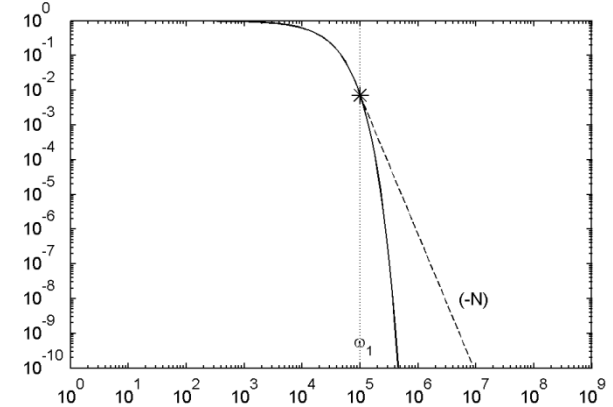

Fig. 14. Auxiliary magnitude function used for determining $\tilde{\varphi}_{mps}$.
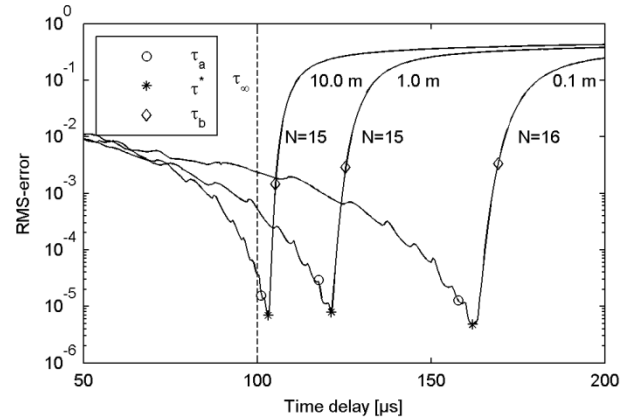
Fig. 15. Bracketing intervals [τ_a, τ_b] and identified optimum τ^* using auxiliary magnitude function and golden section search, with prescribed RMS-error of $\varepsilon = 10^{-5}$.

D. Estimation of Left Bracket With Given Model Order

In other situations, only the model order may be known without requirements for the RMS-error. The concept of an auxiliary function in Fig. 15 may also be used in this case. It is only required that the evaluation frequency ω_1 is chosen such that the value $|H(\omega_1)|$ is smaller than the expected model error, or equal to the upper frequency limit of the fitting band if this condition cannot be met.

E. Pseudo-Code for Delay Optimization

The steps for delay optimization are summarized in Fig. 16, assuming that a specified error level is used.

Input:
- Target error, ε.
- |H(ω)| at logarithmically spaced frequencies
- Number of frequency decades to be used, N_{dec}.

Determine evaluation frequency, $\underline{\omega_1}$:
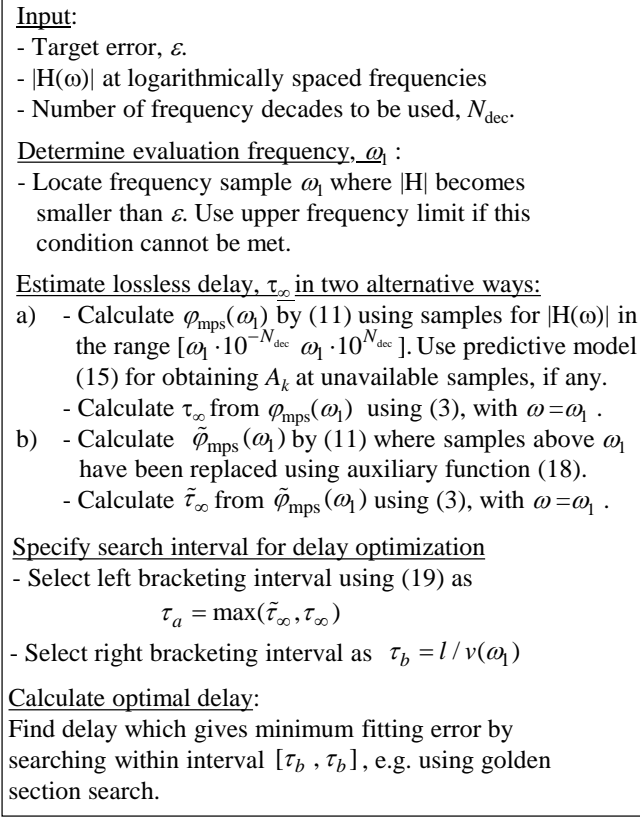- Locate frequency sample ω_1 where |H| becomes smaller than ε. Use upper frequency limit if this condition cannot be met.

Estimate lossless delay, τ_∞ in two alternative ways:
a) - Calculate $\varphi_{\mathrm{mps}}(\omega_1)$ by (11) using samples for |H(ω)| in the range [$\omega_1 \cdot 10^{-N_{\mathrm{dec}}}$ $\omega_1 \cdot 10^{N_{\mathrm{dec}}}$]. Use predictive model (15) for obtaining A_k at unavailable samples, if any.
    - Calculate τ_∞ from $\varphi_{\mathrm{mps}}(\omega_1)$ using (3), with $\omega = \omega_1$.
b) - Calculate $\tilde{\varphi}_{\mathrm{mps}}(\omega_1)$ by (11) where samples above ω_1 have been replaced using auxiliary function (18).
    - Calculate $\tilde{\tau}_\infty$ from $\tilde{\varphi}_{\mathrm{mps}}(\omega_1)$ using (3), with $\omega = \omega_1$.

Specify search interval for delay optimization
- Select left bracketing interval using (19) as
$$\tau_a = \max(\tilde{\tau}_\infty, \tau_\infty)$$
- Select right bracketing interval as $\tau_b = l / v(\omega_1)$

Calculate optimal delay:
Find delay which gives minimum fitting error by searching within interval [τ_b , τ_b], e.g. using golden section search.

Fig. 16. Steps in delay optimization.

IX. EXAMPLE: CABLE MODELING

As an application example, consider the cable system in Fig. 17 with parameters given in Table VI. Fig. 18 shows the magnitudes of the six modes of propagation. The left bracket for the search interval is calculated as described in Sections VIII-B and VIII-C with $\varepsilon = 10^{-4}$.

Fig. 19 shows the fitting results for the ground mode (H_1), two inter-sheath modes (H_2, H_3), and one of the coaxial modes (H_4). The true minima are seen to be located inside the pre-calculated intervals and identified using golden section search.
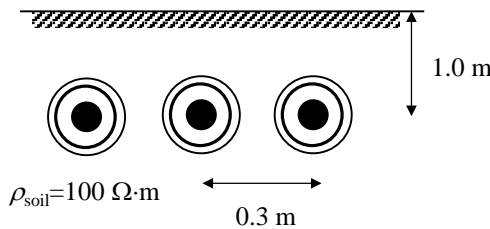

Fig. 17. Cable system.

$\rho_{\mathrm{soil}} = 100\ \Omega\cdot m$

1.0 m

0.3 m

TABLE VI.
SC CABLE DATA.

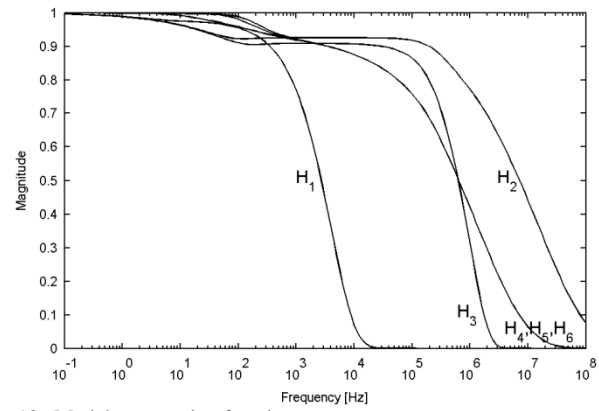| Item	Property
Core	OD=39 mm , ρ= 3.365E–8 $\Omega\cdot$m
Insulation	t=18.25 mm , ε_r=2.85
Sheath	t=0.22 mm , ρ= 1.718E–8 $\Omega\cdot$m
Jacket	t=4.53 mm, ε_r=2.51

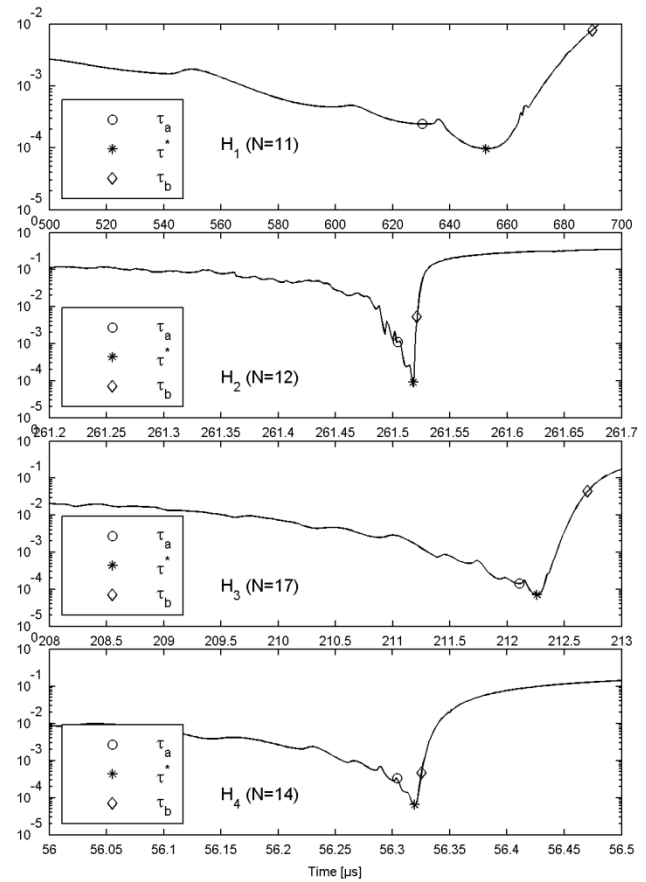
Fig. 18. Modal propagation functions.

Fig. 19. RMS-error when fitting modal propagation functions with required accuracy of 1E–4.

X. DISCUSSION

In practice, the CPU time of the delay calculation is dominated by the final optimization where a rational model must be fitted to the propagation function repeatedly. In most implementations of ULM in EMTP-type programs, the user specifies a target for the fitting error. The program starts with a low-order approximation and increases the order n_1 times until the target error is reached. For each order, delay optimization is used which results in n_2 calls to the fitter, which is usually vector fitting (VF). Since VF is based on iteratively relocating poles to better positions, another n_3 calls to VF is needed for the poles to converge. Although VF is

very fast and requires only a fraction of a second to evaluate, the use of $n_1 \cdot n_2 \cdot n_3$ calls can make the whole process take a few seconds which can be an issue for a simulation case which involves many overhead lines and cables. It is therefore of practical interest to reduce the number of iteration steps n_2 in the optimization as much as possible. Such reduction of n_2 is achieved by using a narrow search interval and a good procedure for optimization. In the first development of ULM [9], a simple search procedure was adopted as shown in Fig. 20 with initial step length chosen equal to half the interval length, Δ. That approach is more robust than Golden section search (Section VII.B) as it will also search outside the bracketing interval if necessary. However, the step length is less optimal and so it generally needs more steps to locate the optimum. Also, the additional robustness is not needed if the bracketing interval has been calculated in a reliable way. Another option is Brent's method as applied in [14]. That approach requires even fewer steps by combining Golden section search with a parabolic local model. .

```
for n=1:N_G
    rmserr_0 = fit(poles,tau_n)
    for iter=1:Niter
        tau_n = tau_n +Δ
        rmserr = fit(poles,tau_n)
        if rmserr > rmserr_0
            Δ=-Δ/2
        end
        rmserr_0=rmserr
    end
end
```

Fig. 20. Alternative method for locating the delay optimum [18].

XI. CONCLUSION

In the Universal Line Model (ULM), the modeling of the propagation function with rational functions requires precalculation of the time delays. In current ULM implementations, the delay calculation is based on estimating the lossless delay τ_∞ from the minimum-phase-shift angle associated with the propagation magnitude function, followed by an optimization process.

This paper derives the discrete integral formula that was used in the first implementation of ULM for estimating the lossless delay τ_∞, showing that it has an error. When using the corrected formula, a very precise estimation of τ_∞ is achieved. Application to a synthetic example with given frequency resolution shows that the accuracy of the corrected formula is even higher than that by direct application of Bode's classical formula.

One significant source of error in practical applications is the truncation effects due to the finite upper frequency limit. It is shown that by using a predictive model of the out-of-band samples, truncation effects on the estimated τ_∞ can be substantially reduced.

The lossless time delay is not the optimal time delay to be used when the objective is to minimize the fitting error. It is demonstrated that the optimal delay can be substantially bigger than the lossless delay, in particular for overhead conductors in close proximity to earth. It is therefore necessary to search for the optimal delay within a bracketing interval, which is also the practice in the current implementations of ULM. This paper shows that the search interval can be made substantially more narrow by introducing an auxiliary magnitude function that restricts the high-frequency phase shift to comply with the maximum phase shift that can be supported by the rational model.

XII. REFERENCES

[1] *EMTP Theory Book*, prepared by H.W. Dommel. Bonneville Power Administration, Portland, Oregon, U.S.A. August 1986.
[2] L.M. Wedepohl, "Transient analysis of underground power-transmission systems. System-model and wave-propagation characteristics", *Proc. IEE*, vol. 120, no. 2, pp. 253-260, February 1973.
[3] A. Ametani, "A general formulation of impedance and admittance of cables", *IEEE Trans. Power Apparatus and Systems*, vol. 99, no. 3, pp. 902-910, 1980.
[4] A. Semlyen and A. Dabuleanu, "Fast and accurate switching transient calculations on transmission lines with ground return using recursive convolutions", *IEEE Trans. Power Apparatus and Systems*, vol. 94, pp. 561-575, March/April 1975.
[5] J.R. Marti, "Accurate modelling of frequency-dependent transmission lines in electromagnetic transient simulations", *IEEE Trans. Power Apparatus and Systems*, vol. 101, no. 1, pp. 147-157, January 1982.
[6] L. Marti, "Simulation of transients in underground cables with frequency-dependent modal transformation matrices" *IEEE Trans. Power Delivery*, vol. 3, no. 3, pp. 1099-1110, July 1988.
[7] B. Gustavsen and A. Semlyen, "Simulation of transmission line transients using vector fitting and modal decomposition", *IEEE Trans. Power Delivery*, vol. 13, no. 2, pp. 605-614, August 2002.
[8] A. Morched, B. Gustavsen, and M. Tartibi, "A universal model for accurate calculation of electromagnetic transients on overhead lines and underground cables", *IEEE Trans. Power Delivery*, vol. 14, no. 3, pp. 1032-1038, July 1999.
[9] B. Gustavsen, G. Irwin, R. Mangelrød, D. Brandt, and K. Kent, "Transmission line models for the simulation of interaction phenomena between parallel AC and DC overhead lines", *Proc*. International Conference on Power Systems Transients (IPST), Budapest, Hungary, June 20-24, 1999, pp. 61-67.
[10] B. Gustavsen and A. Semlyen, "Rational approximation of frequency domain responses by vector fitting", *IEEE Trans. Power Delivery*, vol. 14, no. 3, pp. 1052-1061, July 1999.
[11] B. Gustavsen, "Improving the pole relocating properties of vector fitting", *IEEE Trans. Power Delivery*, vol. 21, no. 3, pp. 1587-1592, July 2006.
[12] I. Kocar and J. Mahseredjian, "New procedure for computation of time delays on propagation functions for transient modeling of cables", *IEEE Trans. Power Delivery*, available online: ieeeXplore.
[13] H.W. Bode, *Network analysis and feedback amplifier design*, D. Van Nostrand, New York, 1945.
[14] B. Gustavsen, "Time delay identification for transmission line modeling", *Proc*. 8th IEEE Workshop on Signal Propagation on Interconnects Heidelberg, Germany, pp. 103-106, May 9-12, 2004.
[15] H.W. Bode, *Network analysis and feedback amplifier design*, D. Van Nostrand, New York, 1945.
[16] Jens G. Balchen, *Reguleringsteknikk. Bind 1*, Tapir Forlag, 1984.
[17] W. Press, S. Reukolsky, W. Vetterling, B. Flannery, *Numerical recipes*, Cambridge University Press, third edition, 2007.
[18] B. Gustavsen, and J. Nordstrom, "Pole identification for the universal line model based on trace fitting", *IEEE Trans. Power Delivery*, vol. 23, no. 1, pp. 472-479, January 2008.

XIII. BIOGRAPHY

Bjørn Gustavsen (M'94–SM'2003–F'2014) was born in Norway in 1965. He received the M.Sc. degree and the Dr.Ing. degree in Electrical Engineering from the Norwegian Institute of Technology (NTH) in Trondheim, Norway, in 1989 and 1993, respectively. Since 1994 he has been working at SINTEF Energy Research where he is currently Chief Scientist. His interests include simulation of electromagnetic transients and modeling of frequency dependent effects.